

## Cluster compounds | Hot Paper |

Atomically Precise Lanthanide-Iron-Oxo Clusters Featuring the  $\epsilon$ -Keggin IonXiu-Ying Zheng,<sup>[a, b]</sup> Ming-Hao Du,<sup>[a]</sup> Mehran Amiri,<sup>[c]</sup> May Nyman,<sup>\*[c]</sup> Qiang Liu,<sup>[d]</sup> Tao Liu,<sup>[d]</sup> Xiang-Jian Kong,<sup>\*[a]</sup> La-Sheng Long,<sup>\*[a]</sup> and Lan-Sun Zheng<sup>[a]</sup>

**Abstract:** Atomically precise molecular metal-oxo clusters provide ideal models to understand metal oxide surfaces, self-assembly, and form-function relationships. Devising strategies for synthesis and isolation of these molecular forms remains a challenge. Here, the synthesis of four Ln-Fe oxo clusters that feature the  $\epsilon$ -{Fe<sub>13</sub>} Keggin cluster in their core is reported. The {Fe<sub>13</sub>} metal-oxo cluster motif is the building block of two important iron oxyhydroxide phases in nature and technology, ferrihydrite (as the  $\delta$ -isomer) and magnetite (the  $\epsilon$ -isomer). The reported  $\epsilon$ -{Fe<sub>13</sub>} Keggin isomer as an isolated molecule provides the opportunity to study the formation of ferrihydrite and magnetite from this building unit. The four currently reported isostructural lanthanide-iron-oxo clusters are fully formulated [Y<sub>12</sub>Fe<sub>33</sub>(TEOA)<sub>12</sub>(Hyp)<sub>6</sub>( $\mu_3$ -OH)<sub>20</sub>( $\mu_4$ -O)<sub>28</sub>(H<sub>2</sub>O)<sub>12</sub>](ClO<sub>4</sub>)<sub>23</sub>·50 H<sub>2</sub>O (**1**, Y<sub>12</sub>Fe<sub>33</sub>), [Gd<sub>12</sub>Fe<sub>33</sub>(TEOA)<sub>12</sub>(Hyp)<sub>6</sub>( $\mu_3$ -OH)<sub>20</sub>( $\mu_4$ -O)<sub>32</sub>(H<sub>2</sub>O)<sub>12</sub>]-

(ClO<sub>4</sub>)<sub>15</sub>·50 H<sub>2</sub>O (**2**, Gd<sub>12</sub>Fe<sub>33</sub>) and [Ln<sub>16</sub>Fe<sub>29</sub>(TEOA)<sub>12</sub>(Hyp)<sub>6</sub>( $\mu_3$ -OH)<sub>24</sub>( $\mu_4$ -O)<sub>28</sub>(H<sub>2</sub>O)<sub>16</sub>](ClO<sub>4</sub>)<sub>16</sub>(NO<sub>3</sub>)<sub>3</sub>·*n* H<sub>2</sub>O (Ln = Y for **3**, Y<sub>16</sub>Fe<sub>29</sub>, *n* = 37 and Ln = Gd for **4**, Gd<sub>16</sub>Fe<sub>29</sub>, *n* = 25; Hyp = *trans*-4-Hydroxyl-L-proline and TEOA = triethanolamine). The next metal layer surrounding the  $\epsilon$ -{Fe<sub>13</sub>} core within these clusters exhibits a similar arrangement as the magnetite lattice, and Fe and Ln can occupy the same positions. This provides the opportunity to construct a family of compounds and optimize magnetic exchange in these molecules through composition tuning. Small-angle X-ray scattering (SAXS) and high-resolution electrospray ionization mass spectrometry (HRESI-MS) show that these clusters are stable upon dissolution in both water and organic solvents, as a first step to performing further chemistry towards building magnetic arrays or investigating ferrihydrite and magnetite assembly from pre-nucleation clusters.

## Introduction

Iron oxides and hydroxides are the most abundant of the transition metal oxides in nature. They play important roles in envi-

ronmental geology, biomineralization, microbiological activity, magnetic materials and other related fields.<sup>[1]</sup> Important iron oxide minerals include haematite ( $\alpha$ -Fe<sub>2</sub>O<sub>3</sub>), magnetite (Fe<sub>3</sub>O<sub>4</sub>), goethite ( $\alpha$ -FeOOH), lepidocrocite ( $\gamma$ -FeOOH), and ferrihydrite (Fe<sub>5</sub>HO<sub>8</sub>·4H<sub>2</sub>O).<sup>[2]</sup> The basic structural unit in these iron oxides is the FeO<sub>6</sub> or FeO<sub>3</sub>(OH)<sub>3</sub> octahedron and the FeO<sub>4</sub> tetrahedron. In the structure of magnetite, a tetrahedron is surrounded by twelve edge-sharing octahedra, resembling the molecular  $\epsilon$ -Keggin-Fe<sub>13</sub> structure.<sup>[3]</sup> Magnetite has many applications in magnetic materials, catalytic and medical sciences (magnetic resonance imaging, MRI).<sup>[4]</sup>

In addition, a structural model has been proposed for ferrihydrite that also contains the Keggin structure ( $\delta$ -Keggin-Fe<sub>13</sub>). However, this structure and even the existence of tetrahedral iron in ferrihydrite is a subject of ongoing debate.<sup>[5]</sup> Ferrihydrite, central to contaminant transport,<sup>[6]</sup> microbe metabolism and iron cycling,<sup>[7]</sup> is one of the most prominent minerals in the biogeosphere; ubiquitous in soils, acid mine drainage, and ferritin.<sup>[8]</sup>


Recently, some of us isolated atomically precise iron-oxo clusters of the  $\alpha$ -Fe<sub>13</sub>-Keggin structural motif, closely related to the structural building blocks of magnetite and ferrihydrite. It was accomplished by use of Bi<sup>3+</sup> to stabilize the hydrolytically reactive cluster. In addition, we demonstrated room temperature conversion of the molecular  $\alpha$ -Fe<sub>13</sub> to ferrihydrite,<sup>[9]</sup> and to magnetite with chemical reduction.<sup>[10]</sup> Both processes involved

[a] X.-Y. Zheng, M.-H. Du, Prof. Dr. X.-J. Kong, Prof. Dr. L.-S. Long, Prof. Dr. L.-S. Zheng  
Collaborative Innovation Center of Chemistry for Energy Materials  
State Key Laboratory of Physical Chemistry of Solid Surfaces and  
Department of Chemistry, College of Chemistry and Chemical Engineering  
Xiamen University, Xiamen, 361005 (P. R. China)  
E-mail: xjkong@xmu.edu.cn  
lslong@xmu.edu.cn

[b] X.-Y. Zheng  
Institutes of Physical Science and Information Technology  
Key Laboratory of Structure and Functional Regulation of  
Hybrid Materials of Ministry of Education  
Anhui University, Hefei, 230601 (P. R. China)

[c] M. Amiri, Prof. Dr. M. Nyman  
Department of Chemistry  
Oregon State University  
Corvallis, 97331 (USA)  
E-mail: may.nyman@oregonstate.edu

[d] Q. Liu, Prof. Dr. T. Liu  
State Key Laboratory of Fine Chemicals  
Dalian University of Technology  
Dalian, 116024 (P. R. China)

 Supporting information and the ORCID identification number(s) for the author(s) of this article can be found under:  
<https://doi.org/10.1002/chem.201904636>

deliberate removal of the capping bismuth. While these studies provided insight into the viability of the molecular Keggin cluster as a predecessor to related materials, the origin of structural differences between the isolated  $\alpha$ - $\text{Fe}_{13}$  molecule and the Keggin-structure building units of ferrihydrite ( $\delta$ -isomer) and magnetite ( $\varepsilon$ -isomer) are still not understood. There are a total of five aforementioned isomers of the Keggin-structure:  $\alpha$ ,  $\beta$ ,  $\gamma$ ,  $\delta$  and  $\varepsilon$ . All have a central tetrahedron surrounded by four sets of three edge-sharing octahedra (trimers). The linkage between the trimers defines the isomers, and they are related to each other by 60-degree rotations of the trimer, about the Fe–O bond axis of the tetrahedron (Figure 1). Consequently, all trimers are corner-sharing in the  $\alpha$ -isomer ( $T_d$  symmetry) and  $\beta$ -isomer ( $C_{3v}$  symmetry). The  $\gamma$ -isomer has two trimers corner-linked and two edge-linked ( $C_{2v}$ ). The  $\delta$ -isomer is also  $C_{3v}$  symmetry, with three trimers edge-sharing and the fourth corner-linked. Finally, the  $\varepsilon$ -isomer features all edge-sharing between trimers, and a return to  $T_d$  symmetry. Because the  $\alpha$ -isomer differs from the  $\delta$  and  $\varepsilon$  isomers, an isolated molecule that more closely resembles the related material would advance our understanding of its importance in mineral and materials self-assembly, as well as provide crucial models for spectroscopic investigations of poorly crystalline ferrihydrite.<sup>[11]</sup>

Herein, we have expanded the strategy of iron-oxo cluster stabilization to rare-earths to stabilize the  $\text{Fe}_{13}$ -cluster, along with amino acid ligands. In the four structures described here,  $\text{Y}^{3+}/\text{Gd}^{3+}$  or additional  $\text{Fe}^{3+}$  ions stabilize an  $\text{Fe}_{13}$ -core with the  $\varepsilon$ -topology. The  $\varepsilon$ - $\{\text{Fe}_{13}\}$  motif has been observed only once before in the molecular form, capped with four additional Fe–Cl units and pyridine ligands.<sup>[3a]</sup> Lanthanide ions further broaden the utility of Fe-oxo clusters including single-molecule magnets for information storage,<sup>[12]</sup> magnetic refrigeration materi-

als with high magnetocaloric effects,<sup>[13]</sup> and developing an understanding of magnetic exchange interactions.<sup>[14]</sup>

Employing ligands *trans*-4-Hydroxyl-L-proline (Hyp) and triethanolamine (TEOA- $\text{H}_3$ ), we isolated  $[\text{Y}_{12}\text{Fe}_{33}(\text{TEOA})_{12}(\text{Hyp})_6(\mu_3\text{-OH})_{20}(\mu_4\text{-O})_{28}(\text{H}_2\text{O})_{12}](\text{ClO}_4)_{23}\cdot 50\text{H}_2\text{O}$  (**1**,  $\text{Y}_{12}\text{Fe}_{33}$ ),  $[\text{Gd}_{12}\text{Fe}_{33}(\text{TEOA})_{12}(\text{Hyp})_6(\mu_3\text{-OH})_{20}(\mu_4\text{-O})_{32}(\text{H}_2\text{O})_{12}](\text{ClO}_4)_{15}\cdot 50\text{H}_2\text{O}$  (**2**,  $\text{Gd}_{12}\text{Fe}_{33}$ ),  $[\text{Y}_{16}\text{Fe}_{29}(\text{TEOA})_{12}(\text{Hyp})_6(\mu_3\text{-OH})_{24}(\mu_4\text{-O})_{28}(\text{H}_2\text{O})_{16}](\text{ClO}_4)_{16}(\text{NO}_3)_3\cdot 37\text{H}_2\text{O}$  (**3**,  $\text{Y}_{16}\text{Fe}_{29}$ ) and  $[\text{Gd}_{16}\text{Fe}_{29}(\text{TEOA})_{12}(\text{Hyp})_6(\mu_3\text{-OH})_{24}(\mu_4\text{-O})_{28}(\text{H}_2\text{O})_{16}](\text{ClO}_4)_{16}(\text{NO}_3)_3\cdot 25\text{H}_2\text{O}$  (**4**,  $\text{Gd}_{16}\text{Fe}_{29}$ ). While TEOA has been used extensively in isolating iron-oxo clusters,<sup>[15]</sup> proline has been more scarcely exploited in this role.<sup>[16]</sup> Single-crystal structure analysis shows that these 45-metal cluster compounds **1–4** are the largest lanthanide-iron-oxo clusters to date, and all the 45 metal ions in the cores of **1–4** possess the same  $\varepsilon$ - $\text{Fe}_{13}$  metal arrangement that is observed in magnetite (Figures 1 a–c). While the  $\varepsilon$ - $\text{Fe}_{13}$  core is a commonality of all described molecules, there is flexibility in the outer 33 metal ions, where Ln can directly replace Fe in these isostructural compounds. From these reported structures and the previously described Bi-capped  $\text{Fe}_{13}$ , we can start to develop design rules (capping metals and ligands) for stabilizing clusters of different topologies that are important in understanding materials assembly from pre-nucleation clusters. In addition, ferrihydrite controls the fractionation transport of many minor elements in the environment including rare-earths, and conversely the minor elements alter the conversion of ferrihydrite to other mineral phases.<sup>[17]</sup> Therefore, these phases can serve as models for these processes in nature that are important in considering rare-earth mining. Small angle X-ray scattering (SAXS) and high-resolution electrospray ionization mass spectrometry (HRESI-MS) show the stability of these clusters in both water and organic solvents. This is an important first step for future solution phase manipulation and conversion to related materials.

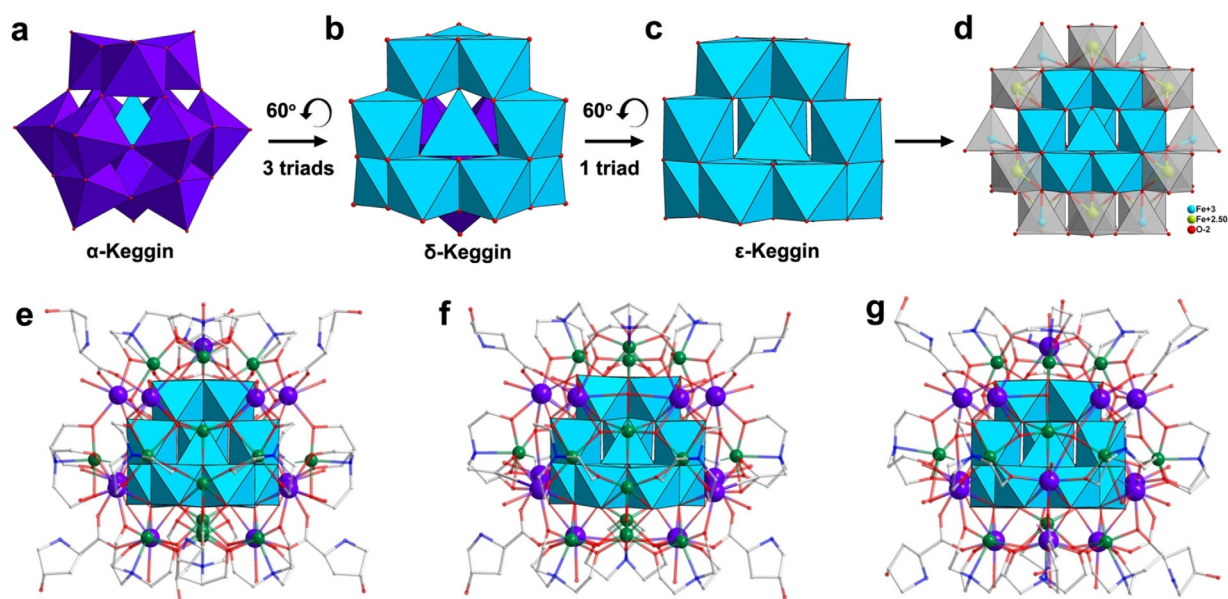


**Figure 1.** Polyhedral representation of the crystal structures of the isomers of the Keggin anion. (a) The  $\alpha$ -type, (b)  $\delta$ -type Keggin and (c)  $\varepsilon$ -type Keggin structure; (d) The  $\varepsilon$ -Keggin iron ion in magnetite; The cationic cluster core of (e)  $\text{Y}_{12}\text{Fe}_{33}$ , (f)  $\text{Gd}_{12}\text{Fe}_{33}$  and (g)  $\text{Ln}_{16}\text{Fe}_{29}$  ( $\text{Ln} = \text{Y}$  and  $\text{Gd}$ ). C, grey; O, red; N, blue; Ln, purple; Fe, green. H atoms omitted for clarity.

## Results and Discussion

### Synthesis and structures of compounds 1–4

In this work, lanthanide ions, *trans*-4-Hydroxyl-L-proline (Hyp) and triethanolamine (TEOA-H<sub>3</sub>) were introduced to control the hydrolysis of iron ions and stabilize the formed molecular clusters. When changing the type and concentration of anions, some Ln<sup>3+</sup> ions in Ln<sub>12</sub>Fe<sub>33</sub> are replaced by Fe<sup>3+</sup> ions and form isotypical clusters Ln<sub>16</sub>Fe<sub>29</sub>. Single-crystal X-ray diffraction reveals that Ln<sub>12</sub>Fe<sub>33</sub> and Ln<sub>16</sub>Fe<sub>29</sub> display the same metal arrangement, with facile replacement of Ln to Fe onto the core structure (Figures 1 e–f). The yields of the structures presented below are ≈30%, and the same formulations (i.e., Ln:Fe ratio and arrangement of the metals) is consistent in repeated reactions, as indicated by magnetic and mass spectroscopy data, discussed later. We believe there could be other cluster assemblages present in solution that do not readily crystallize and represent opportunity for future isolation. Y<sub>12</sub>Fe<sub>33</sub> crystallizes in the tetragonal space group *I*<sub>4</sub>/*amd*, whereas Gd<sub>12</sub>Fe<sub>33</sub> crystallizes in the hexagonal space group *P*6<sub>3</sub>/*mcm*. Y<sub>16</sub>Fe<sub>29</sub> and Gd<sub>16</sub>Fe<sub>29</sub> are isostructural and crystallized in the trigonal space group *R* $\bar{3}$ c. As an example, only Y<sub>12</sub>Fe<sub>33</sub> is described below in detail.

The compound Y<sub>12</sub>Fe<sub>33</sub> can be described as {[Fe<sub>13</sub>(μ<sub>3</sub>-OH)<sub>12</sub>(μ<sub>4</sub>-O)<sub>28</sub>]<sub>2</sub>[Y<sub>12</sub>Fe<sub>20</sub>(TEOA)<sub>12</sub>(Hyp)<sub>6</sub>(μ<sub>3</sub>-OH)<sub>8</sub>(H<sub>2</sub>O)<sub>12</sub>]<sub>2</sub>}<sup>23+</sup>, centred by the ε-Keggin type {Fe<sub>13</sub>} anion (Figure 1 e). As shown in Figure 2 a, the ε-Keggin iron oxoanion formulated as [Fe<sub>13</sub>(μ<sub>3</sub>-OH)<sub>12</sub>(μ<sub>4</sub>-O)<sub>28</sub>]<sup>29-</sup> can be viewed as four-vertex μ<sub>4</sub>-O<sup>2-</sup> groups on the tetrahedral unit [Fe(μ<sub>4</sub>-O)<sub>4</sub>]<sup>5-</sup> (Fe–O = 1.864(4) Å), that links to a trimer of edge-sharing hexa-coordinate Fe<sup>3+</sup> ions. Interestingly, hydroxyl ligands occupy the terminal positions of the

central Keggin ion (Figure S1 in Supporting Information, the bond valence sum calculations in Table S1). In contrast, in the previously described α-Fe<sub>13</sub>,<sup>[9]</sup> hydroxyls occupy the μ<sub>2</sub>-bridging sites within the edge-sharing trimers of the Keggin ion, and oxos link the trimers by corner-sharing. Each hexa-coordinate Fe<sup>3+</sup> ion in {ε-Fe<sub>13</sub>} is formulated [Fe(μ<sub>3</sub>-OH)(μ<sub>4</sub>-O)<sub>5</sub>]<sup>8-</sup> (Figure S2 a). Three octahedral units [Fe(μ<sub>3</sub>-OH)(μ<sub>4</sub>-O)<sub>5</sub>]<sup>8-</sup> form edge-sharing triads [Fe<sub>3</sub>(μ<sub>3</sub>-OH)<sub>3</sub>(μ<sub>4</sub>-O)<sub>7</sub>]<sup>8-</sup> (Figure S2 b). Four octahedral-triad units are connected by edge-sharing (Figure S2 c), which further link with the central tetrahedral [Fe(μ<sub>4</sub>-O)<sub>4</sub>]<sup>5-</sup> through the four μ<sub>4</sub>-O<sup>2-</sup> groups. As shown in Figure 2 b, four square pyramidal units [Fe(μ<sub>3</sub>-OH)<sub>2</sub>(μ<sub>4</sub>-O)<sub>3</sub>]<sup>5-</sup> connect to the vertices of four octahedral-triads [Fe<sub>3</sub>(μ<sub>3</sub>-OH)<sub>3</sub>(μ<sub>4</sub>-O)<sub>7</sub>]<sup>8-</sup> units through three μ<sub>4</sub>-O<sup>2-</sup> groups, thus producing the larger iron-oxo cluster unit [Fe<sub>17</sub>(μ<sub>3</sub>-OH)<sub>20</sub>(μ<sub>4</sub>-O)<sub>28</sub>]<sup>25-</sup> (Figure 2 c). These square-pyramidal iron-centres sit in the hexagonal “window” of the ε-Fe<sub>13</sub> core. Notably, this is the same location as the next layer of polyhedra of the Keggin unit in both ferrihydrite and magnetite. In addition, twelve yttrium ions Y<sup>3+</sup> and four other iron ions further cap on the ε-Keggin anion [Fe<sub>13</sub>(μ<sub>3</sub>-OH)<sub>12</sub>(μ<sub>4</sub>-O)<sub>28</sub>]<sup>29-</sup> through μ<sub>3</sub>-OH<sup>-</sup> and μ<sub>4</sub>-O<sup>2-</sup> groups, thereby generating a cage-like lanthanide-iron-oxo cluster unit [Y<sub>12</sub>Fe<sub>21</sub>(μ<sub>3</sub>-OH)<sub>20</sub>(μ<sub>4</sub>-O)<sub>28</sub>]<sup>23+</sup> (Figure 2 d). The cationic cluster unit [Y<sub>12</sub>Fe<sub>21</sub>(μ<sub>3</sub>-OH)<sub>20</sub>(μ<sub>4</sub>-O)<sub>28</sub>]<sup>23+</sup> is further protected and stabilized by twelve neutral chelate [Fe(TEOA)] units (Figure 2 e), thus forming a chelated cluster [Y<sub>12</sub>Fe<sub>33</sub>(TEOA)<sub>12</sub>(μ<sub>3</sub>-OH)<sub>20</sub>(μ<sub>4</sub>-O)<sub>28</sub>]<sup>23+</sup> (Figure 2 f). This cluster unit is then protected and stabilized by six organic Hyp ligands and twelve coordinated water molecules, producing the cationic cluster unit [Y<sub>12</sub>Fe<sub>33</sub>(TEOA)<sub>12</sub>(Hyp)<sub>6</sub>(μ<sub>3</sub>-OH)<sub>20</sub>(μ<sub>4</sub>-O)<sub>28</sub>(H<sub>2</sub>O)<sub>12</sub>]<sup>23+</sup>. From the structural profile, it may be speculated that Y<sub>12</sub>Fe<sub>33</sub> has a process of growing from inside to outside. Firstly, the Fe<sub>13</sub> core was formed by the hydrolysis of Fe<sup>3+</sup> ions. Second, due to the hydrolysis and coordination ability of Y<sup>3+</sup> ions, it competes with Fe<sup>3+</sup> ions in solution, thus preventing aggregation of the Fe<sub>13</sub> intermediate by occupying the sites of iron ions. Lastly, the Y<sub>12</sub>Fe<sub>33</sub> was isolated and crystallized independently from solution. This may also serve as a model for incorporation of rare-earths and other impurities into ferrihydrite during its formation.

Molecules or ions displaying the Keggin configuration are found in natural and synthetic materials. In the natural world, the α-Keggin {Al<sub>13</sub>} is the mineral lattice of zunyite,<sup>[18]</sup> and the δ-Keggin {Fe<sub>13</sub>} is the hypothesized building block of ferrihydrite.<sup>[4c,9]</sup> The ε-Keggin iron-oxo ion {Fe<sub>13</sub>} contained in Y<sub>12</sub>Fe<sub>33</sub> can be viewed as a molecular fragment of magnetite. The formula of magnetite can be written as B[AB]O<sub>4</sub> (AB<sub>2</sub>O<sub>4</sub>), which corresponds to Fe<sup>III</sup>[Fe<sup>II</sup>Fe<sup>III</sup>]O<sub>4</sub>. The average valence state of the position for [Fe<sup>II</sup>Fe<sup>III</sup>] is +2.5 because the Fe<sup>III</sup> ions occupy both the tetrahedral and octahedral sites. The A<sup>2+</sup> and B<sup>3+</sup> ions in the formula can be replaced by the atoms having a similar ionic radius or energy level (e.g., Al<sup>3+</sup>, Cr<sup>3+</sup>, Co<sup>2+</sup>, and Mn<sup>2+</sup>) to form new minerals with the same structural configurations but different properties.<sup>[19]</sup> According to Mössbauer spectroscopy (Figures S9, Tables S2–S3, discussed later) and the bond valence sum calculations (Table S4), the iron ions of ε-Keggin {Fe<sub>13</sub>} in Y<sub>12</sub>Fe<sub>33</sub> are all trivalent (Figures 3 a–3b). Interestingly, by comparison, the other metal ions in Y<sub>12</sub>Fe<sub>33</sub> (the remaining

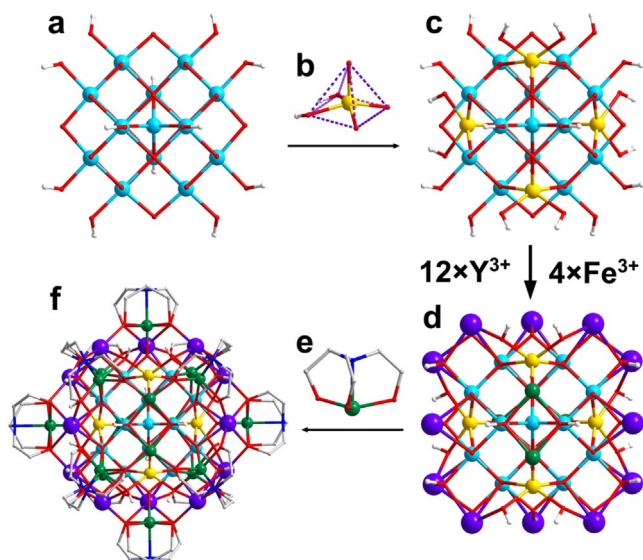


**Figure 2.** The structural analysis diagram of Y<sub>12</sub>Fe<sub>33</sub>. (a) The central iron-oxo ε-Keggin [Fe<sub>13</sub>(μ<sub>3</sub>-OH)<sub>12</sub>(μ<sub>4</sub>-O)<sub>28</sub>]<sup>29-</sup> anion; (b) Square-pyramidal unit [Fe(μ<sub>3</sub>-OH)<sub>2</sub>(μ<sub>4</sub>-O)<sub>3</sub>]<sup>5-</sup>; (c) The iron-oxo cluster [Fe<sub>17</sub>(μ<sub>3</sub>-OH)<sub>20</sub>(μ<sub>4</sub>-O)<sub>28</sub>]<sup>25-</sup>; (d) The cluster unit [Y<sub>12</sub>Fe<sub>21</sub>(μ<sub>3</sub>-OH)<sub>20</sub>(μ<sub>4</sub>-O)<sub>28</sub>]<sup>23+</sup>; (e) The neutral chelates [Fe(TEOA)]; (f) The cationic core [Y<sub>12</sub>Fe<sub>33</sub>(TEOA)<sub>12</sub>(μ<sub>3</sub>-OH)<sub>20</sub>(μ<sub>4</sub>-O)<sub>28</sub>]<sup>23+</sup>. C, grey; O, red; N, blue; Ln, purple; Fe, green/light blue/yellow. H atoms omitted for clarity.

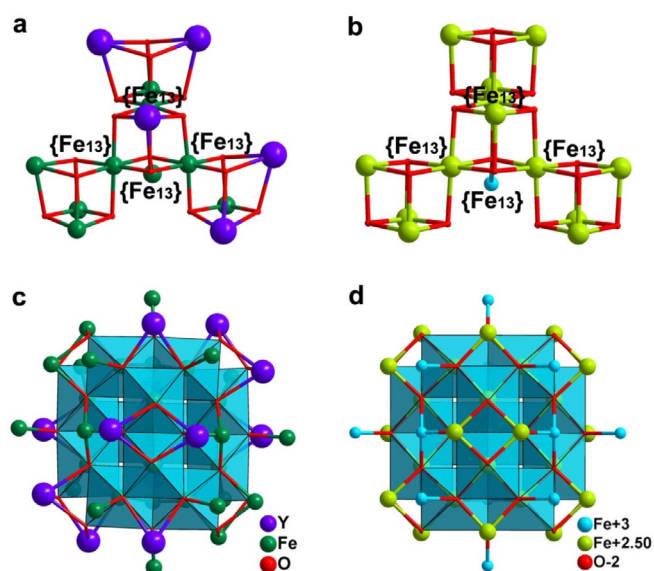


**Figure 3.** The comparison of the metal ion arrangements of  $Y_{12}Fe_{33}$  (a, c) and magnetite (b, d).

$Fe^{3+}$  ions and  $Y^{3+}$  ions) also correspond to the  $Fe^{2.5+}$  and  $Fe^{3+}$  ions positions in magnetite (Figures 3c–3d). That is,  $Y_{12}Fe_{33}$  has the same metal arrangement as magnetite, and in particular, the positions of the  $Y^{3+}$  ions in  $Y_{12}Fe_{33}$  completely correspond to the  $[AB]^{2.5+}$  of  $B[AB]O_4$  in magnetite, as shown in Figure 3. Compared with magnetite, the lanthanide ions indeed occupy part of the iron ion sites and inhibit the continued hydrolysis of iron ions. In summary, this molecular form of magnetite is able to accommodate surface metals that generally require

larger coordination numbers, and the surface curvature allows multidentate ligation.

$Gd_{12}Fe_{33}$  and  $Y_{16}Fe_{29}$  display the same metal topology structure as that of  $Y_{12}Fe_{33}$  (Figures 1e–g), except for some slight differences of the two metal positions. As shown in Figure 4, two  $Y^{3+}$  ions ( $Y1$ ) and two  $Fe^{3+}$  ions ( $Fe1$ ) in  $Y_{12}Fe_{33}$  (Figure 4b) are exchanged by two  $Fe^{3+}$  ions ( $Fe1'$ ) and two  $Gd^{3+}$  ions ( $Gd1'$ ) in  $Gd_{12}Fe_{33}$  (Figure 4d), respectively. The position of the lanthanide ions and iron ions are exchanged due to the different radii between the  $Y^{3+}$  (0.0893 nm) and  $Gd^{3+}$  (0.0938 nm) ions under the same reaction conditions. Meanwhile, the four  $Fe^{3+}$  ion ( $Fe1$ ) positions in  $Y_{12}Fe_{33}$  (Figure 4b) are substituted by four  $Y^{3+}$  ions ( $Y1'$ ) to form  $Y_{16}Fe_{29}$  (Figure 4e). The four penta-coordinate  $Fe^{3+}$  ions featuring the square pyramidal  $[Fe(\mu_3-OH)_2(\mu_4-O)_3]^{5-}$  unit in  $Y_{12}Fe_{33}$  have become hexa-coordinate  $Fe^{3+}$  ions featuring the octahedral unit  $[Fe(\mu_3-OH)_2(\mu_4-O)_4]^{7-}$  in  $Gd_{12}Fe_{33}$  and  $[Fe(\mu_3-OH)_3(\mu_4-O)_3]^{6-}$  in  $Y_{16}Fe_{29}$  (Figure S7), respectively.  $Y_{12}Fe_{33}$ ,  $Gd_{12}Fe_{33}$  and  $Y_{16}Fe_{29}$  have the same central iron-oxo cluster unit  $[Fe_{17}(\mu_3-OH)_{20}(\mu_4-O)_{28}]^{25-}$  that features the same metal ions arrangement as that reported prior for  $\{Fe_{17}\}$  (Figure S8d).<sup>[3]</sup> Furthermore, the neutral chelate  $[Fe(TEOA)]$  unit formed by the  $Fe^{3+}$  ion and deprotonated triethanolamine in 1–4 is invariable and cannot be replaced by lanthanide ions. Structure analysis indicates that the remaining  $Ln^{3+}$  in the structure could potentially be further substituted by the  $Fe^{3+}$  to access other lanthanide-iron-oxo clusters containing different metal ions, or a pure iron-oxo cluster that displays the same metal arrangement as 1–4.

The compounds 1–4 have the same metal skeleton, which can be viewed as the three-shell structure (Figure 4),  $Fe@-$

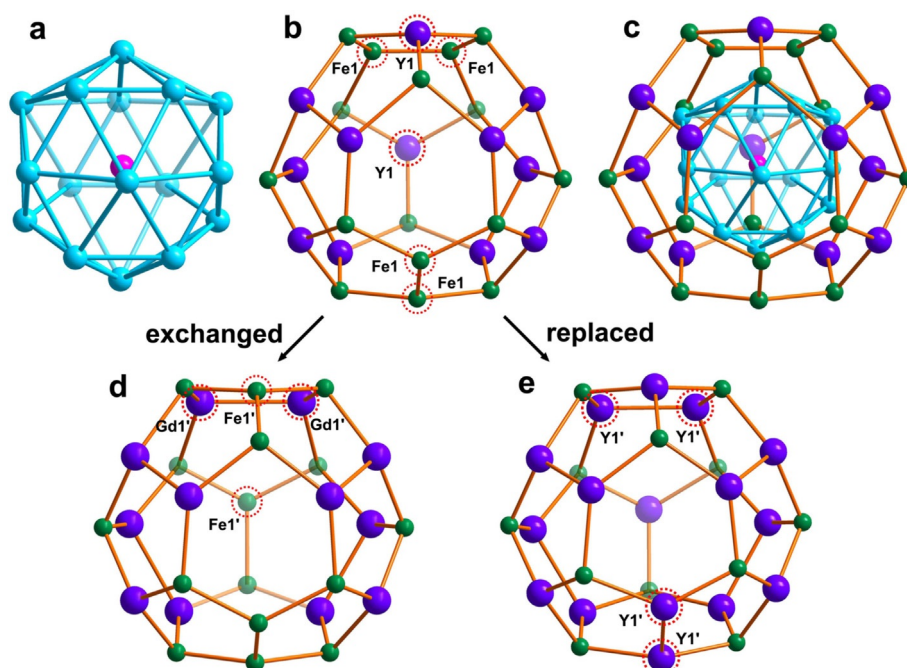


**Figure 4.** The three-shell metal skeleton for  $Y_{12}Fe_{33}$ ,  $Gd_{12}Fe_{33}$  and  $Y_{16}Fe_{29}$ . (a) Double-shell structure  $[Fe@Fe_{16}]$ ; (b) The outermost shell hexadecahedral structure  $\{Y_{12}Fe_{16}\}$  in  $Y_{12}Fe_{33}$ ; (c) The three-shell structure of  $Fe@Fe_{16}@Y_{12}Fe_{16}$  in  $Y_{12}Fe_{33}$ ; (d) The outermost shell  $\{Gd_{12}Fe_{16}\}$  in  $Gd_{12}Fe_{33}$ ; (e) The outermost shell  $\{Y_{16}Fe_{12}\}$  in  $Y_{16}Fe_{29}$ . Ln, purple; Fe, green/light blue/rose.

$\text{Fe}_{16}@\text{Ln}_{12}\text{Fe}_{16}$  ( $\text{Y}_{12}\text{Fe}_{33}$  and  $\text{Gd}_{12}\text{Fe}_{33}$ ) and  $\text{Fe}@\text{Fe}_{16}@\text{Ln}_{16}\text{Fe}_{12}$  ( $\text{Y}_{16}\text{Fe}_{29}$  and  $\text{Gd}_{16}\text{Fe}_{29}$ ). As shown in Figure 4, using  $\text{Y}_{12}\text{Fe}_{33}$  as an example, the innermost shell is only one  $\text{Fe}^{3+}$  ion. Moving outward, the middle shell  $\{\text{Fe}_{16}\}$  consists of 28 triangles  $\{\text{Fe}_3\}$  featuring a cage-like structure (Figure 4a). The outermost shell is a fullerene-like hexadecahedral structure  $\{\text{Y}_{12}\text{Fe}_{16}\}$ , which is composed of 8 pentagons  $\{\text{Y}_3\text{Fe}_2\}$ , 4 pentagons  $\{\text{YFe}_4\}$  and 4 hexagons  $\{\text{Y}_2\text{Fe}_4\}$  (Figure 4b). As displayed in Figures 4d and e, by comparing the metal arrangement of the outermost shell, the differences among them can be seen more clearly.

### Mössbauer spectral studies

The Mössbauer spectra (MS) of the powdered samples of  $\text{Y}_{12}\text{Fe}_{33}$  and  $\text{Gd}_{12}\text{Fe}_{33}$  have been recorded at 78 K. The spectra (Figure 5) show composite quadrupole-split doublets appearing as two broad and asymmetric absorptions for  $\text{Y}_{12}\text{Fe}_{33}$  and  $\text{Gd}_{12}\text{Fe}_{33}$ . For  $\text{Y}_{12}\text{Fe}_{33}$ , to avoid over-parameterization, the spectra were fitted with five doublets based on the crystallographic environments (Figure S10, the environments of Fe2 are similar to Fe4, and those of Fe6 are similar to Fe7). The isomer shift values for the five sites are  $0.354\text{--}0.488\text{ mm s}^{-1}$ , which are expected for high spin  $\text{Fe}^{3+}$  ( $S=5/2$ ) (Table S2).<sup>[20]</sup> The differences in the quadrupole splitting values resulted from a range of bond-length distortions for these  $\text{Fe}^{3+}$  environments. The iron ions for  $\text{Gd}_{12}\text{Fe}_{33}$  can be assigned to six iron sites according to their crystallographic environments (Figure S12). The resulting hyperfine parameters revealed that the fitted isomer shift values of  $0.456\text{--}0.5\text{ mm s}^{-1}$  occurred as expected for high spin  $\text{Fe}^{3+}$  ions (Table S3).<sup>[20b]</sup>

### Small-angle X-ray scattering (SAXS) data

$\text{Gd}_{12}\text{Fe}_{33}$  and  $\text{Gd}_{16}\text{Fe}_{29}$  are soluble in common polar solvents, such as methanol, ethanol, and acetonitrile, as well as highly soluble in water. The dynamic light-scattering (DLS) spectra (Figure S15 in Supporting Information) in water reveal that the

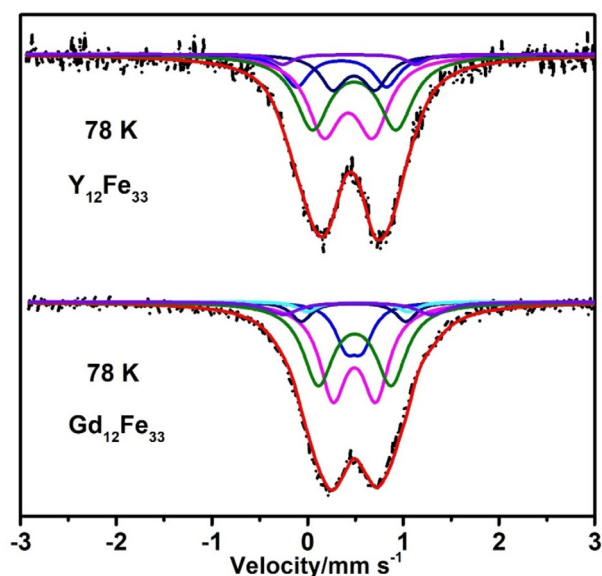


**Figure 5.** Mössbauer spectra of the  $\text{Y}_{12}\text{Fe}_{33}$  and  $\text{Gd}_{12}\text{Fe}_{33}$  obtained at 78 K. The black dashed line and coloured solid lines are the experimental data and the resulting fitting, respectively.

mean hydrodynamic diameter of  $2.4 \pm 0.3\text{ nm}$  is close to that of  $2.5\text{ nm}$  obtained from the crystal data. SAXS provided further detail about the solution behaviour of the clusters. For these studies, we dissolved both  $\text{Gd}_{12}\text{Fe}_{33}$  and  $\text{Gd}_{16}\text{Fe}_{29}$  in acetonitrile, and acetonitrile-methanol mixtures. Interestingly, in pure acetonitrile, none of the three oscillations observed in the simulated scattering data (Figure 6) could be observed in the experimental scattering data (between  $q=0.6\text{--}2.5\text{ \AA}^{-1}$ , Figure S13).<sup>[21]</sup> We found that 10% methanol in acetonitrile allowed observation of the second and third oscillation, but not the first (between  $q=1.0\text{--}2.5\text{ \AA}^{-1}$ , Figure 6), due to both more accurate subtraction of the solvent background (Figure S13) and physical changes in the ligand shell, discussed later. In this solvent mixture, the scattering data features a plateau instead

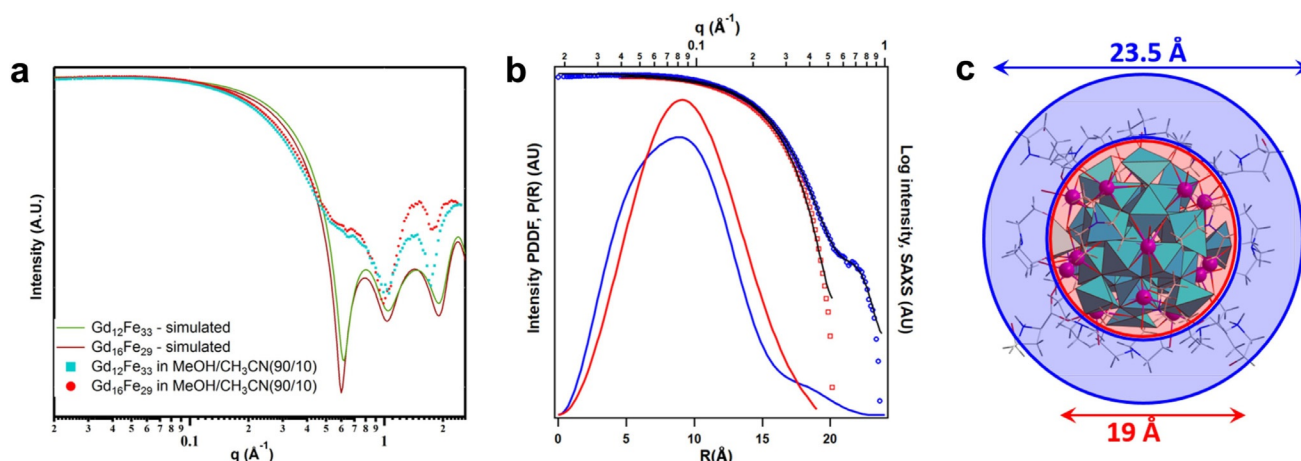


**Figure 6.** (a) Experimental and simulated scattering data for  $\text{Gd}_{12}\text{Fe}_{33}$  and  $\text{Gd}_{16}\text{Fe}_{29}$ ; (b) Pair distance distribution function (PDDF) analyses of  $\text{Gd}_{16}\text{Fe}_{29}$ , both including (blue) and excluding (red) the plateau region of the scattering curve between  $q \approx 0.6\text{--}1.0\text{ \AA}^{-1}$ . The red and blue symbols show the portions of the scattering data that was analysed by PDDF. The black lines are the fits to the data; (c)  $\text{Gd}_{16}\text{Fe}_{29}$  illustrating the metal oxo core representing the red PDDF (excluding the plateau) and the entire cluster representing the blue PDDF (including the plateau).

of the first oscillation of the simulated data, and we deemed this to reflect a real feature of the cluster rather than masking by solvent scattering (discussed below).  $\text{Gd}_{12}\text{Fe}_{33}$  and  $\text{Gd}_{16}\text{Fe}_{29}$  have very similar scattering data, both experimental and simulated. This is expected since they are the same size with the same number of metal centres, where these heavy atoms dominate the scattering intensity. The experimental data is flat below  $q \approx 0.12 \text{ \AA}^{-1}$ , indicative of a monodisperse solution of spherical clusters. Additionally, the match of the 2nd and 3rd oscillations indicates high purity and stability of the clusters.

In the Guinier region ( $q \approx 0.12\text{--}0.5 \text{ \AA}^{-1}$ ), the experimental curves are shifted slightly to lower  $q$  compared to the simulated curves, suggesting a slightly "larger" cluster. To explain this, as well as the unexpected plateau between  $q \approx 0.6\text{--}1.0 \text{ \AA}^{-1}$ , we analysed the scattering data by the pair distance distribution function (PDDF, Figure 6) method of Moore.<sup>[22]</sup> PDDF is a real space representation of the scattering data, and can be described as a probable distribution of scattering vectors through the cluster. PDDF analysis of the scattering data excluding the plateau (Figure 6b, red) gave an approximately Gaussian distribution with a maximum linear extent (diameter, where  $P(R)$  goes to 0) of 19 Å. This is consistent with a spherical cluster with uniform electron density. The second PDDF analysis included the plateau region (Figure 6b, blue) and yielded a major peak (the metal oxo core of the cluster) with a lower intensity "tail" on the high- $R$  side of the peak. This tailing has been observed previously for high electron density cores with lower electron density shells.<sup>[23]</sup> The maximum linear extent is 23 Å, consistent with the diameter of the cluster (including the ligand shell), measured in the X-ray structure. The simulated scattering data with and without the ligand shell is almost identical. This is because the calculation does not "see" any contrast between the ligand shell and the solvent; they both are composed of the light atoms N, C, H and O. However, this shell is clearly denser than the surrounding solvent, impacting the observed scattering data. The above-mentioned shift of the experimental scattering to lower  $q$ , compared to the simulated data is also due to the high-density organic shell that is observed in the experimental data but not the simulated data.

Finally, we believe the addition of methanol to the acetonitrile solution affects the ligand shell, improving the ability to observe the oscillations in the SAXS data, which are very important in identifying monodispersity and purity of dissolved clusters. Highly acidic metal centres (i.e.,  $\text{Ln}^{3+}/\text{Fe}^{3+}$ ) can deprotonate methanol, and methoxy groups will ligate the cluster.<sup>[24]</sup> Methoxy ligands likely replace the water ligands terminating the cluster. This will both add electron density to the solvent shell and trigger a conformation change of the terminally bound ligands. The methanol also aids in solubility; while 10% methanol increases solubility, more results in a decrease in solubility, providing poorer scattering data (Figure S13). In summary, we propose that replacement of water with methanol in the ligand shell leads to a denser ligand shell.

## Electrospray ionization mass spectrometry

In contrast to the previously reported iron-oxo Keggin ion,<sup>[9]</sup> the Ln-Fe clusters  $\text{Y}_{12}\text{Fe}_{33}$  and  $\text{Y}_{16}\text{Fe}_{29}$  are soluble and stable in an aqueous solution. As demonstrated by the high-resolution electrospray ionization mass spectrometry (HRESI-MS) (Figure S14, Table S5), when  $\text{Y}_{12}\text{Fe}_{33}$  was dissolved in ultrapure water under acetonitrile as the diluting solvent condition, a series of  $m/z$  peaks were observed. Two types of five isotopic envelopes with a +3 charge were analysed. As shown in Table S4, the **A1** and **A2** species have the same cationic cluster core of  $[\text{Y}_{12}\text{Fe}_{33}(\text{Hyp})_6(\text{TEOA})_{12}(\text{OH})_{10}(\text{O})_{38}]^{13+}$ , and **B1**, **B2**, and **B3** species display the stable cationic cluster core of  $[\text{Y}_{12}\text{Fe}_{33}(\text{Hyp})_6(\text{TEOA})_{12}(\text{OH})_{11}(\text{O})_{37}]^{14+}$ . The HRESI-MS results reveal that the  $\text{Y}_{12}\text{Fe}_{33}$  metal cationic core is stable, although parts of  $\text{OH}^-$  groups are deprotonated and some solvent molecules are exchanged between  $\text{H}_2\text{O}$  and acetonitrile.<sup>[25]</sup> However the core remains stable over at least ten hours, giving the same peaks by mass spectral analysis. The above results not only demonstrate the stability of the iron-oxo Keggin ion in an aqueous solution but also display the key role of lanthanide ions for stabilizing the Keggin iron oxoanion. A series of lanthanide-iron-oxo clusters with different intermediate structural fragments of magnetite may be obtained by further controlling the reaction conditions to connect different numbers of lanthanide ions or iron ions around the Keggin iron-oxo cluster unit.

## Magnetic studies

The temperature dependence of the magnetic susceptibilities of  $\text{Ln}_{12}\text{Fe}_{33}$  and  $\text{Ln}_{16}\text{Fe}_{29}$  were measured under a 1000 Oe dc field between 2 and 300 K. As shown in Figure 7, at 300 K, the observed  $\chi_{\text{M}}T$  values for  $\text{Y}_{12}\text{Fe}_{33}$ ,  $\text{Gd}_{12}\text{Fe}_{33}$ ,  $\text{Y}_{16}\text{Fe}_{29}$ , and  $\text{Gd}_{16}\text{Fe}_{29}$  are 45.18, 129.59, 34.96 and 140.43  $\text{cm}^3 \text{K mol}^{-1}$ , respectively, which are all much lower than the calculated values based on the isolated  $\text{Fe}^{3+}$  ( $\text{HS Fe}^{3+}$ :  $S=5/2$ ,  $g=2$ ) and  $\text{Gd}^{3+}$  ions ( $\text{Gd}^{3+}$ :  $J=7/2$ ,  $g=2$ ) because of the strong Fe-Fe antiferromagnetic interaction.<sup>[26]</sup> Upon lowering the temperature, the

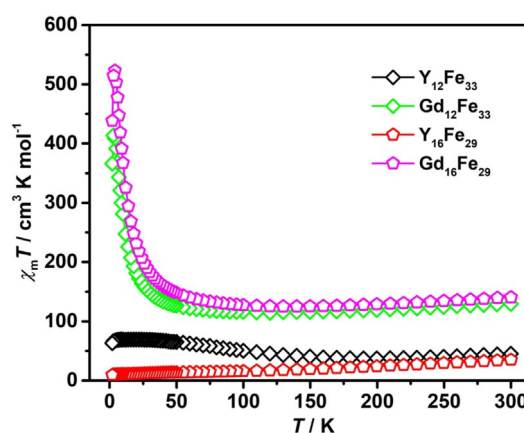


Figure 7. Plots of the temperature dependence of  $\chi_{\text{M}}T$  for  $\text{Y}_{12}\text{Fe}_{33}$ ,  $\text{Gd}_{12}\text{Fe}_{33}$ ,  $\text{Y}_{16}\text{Fe}_{29}$  and  $\text{Gd}_{16}\text{Fe}_{29}$  under  $H_{\text{dc}} = 1000$  Oe.

$\chi_M T$  values for  $Y_{12}Fe_{33}$  decrease to  $37.45 \text{ cm}^3 \text{ K mol}^{-1}$  at 200 K. When further decreasing the temperature, the  $\chi_M T$  value increases to the maximum value of  $69.36 \text{ cm}^3 \text{ K mol}^{-1}$ , and then slowly decreases to  $63.36 \text{ cm}^3 \text{ K mol}^{-1}$  at 2 K. The curve indicated an antiferromagnetic interaction between the iron ions in  $Y_{12}Fe_{33}$ .<sup>[27]</sup> The magnetic susceptibility curves of  $Gd_{12}Fe_{33}$  and  $Gd_{16}Fe_{29}$  show almost the same tendency. With decreasing temperature, the  $\chi_M T$  values gradually decreased to 114.63 and  $125.46 \text{ cm}^3 \text{ K mol}^{-1}$  at 120 K and then rapidly increase to the maximum values of 413.56 and  $523.00 \text{ cm}^3 \text{ K mol}^{-1}$  at 3 K for  $Gd_{12}Fe_{33}$  and  $Gd_{16}Fe_{29}$ , respectively. The  $\chi_M T$  values slightly decrease to 366.05 and  $438.12 \text{ cm}^3 \text{ K mol}^{-1}$  at 2 K, respectively. This result suggested the presence of a ferromagnetic interaction at low temperature between  $Gd^{3+}$  and  $Fe^{3+}$  ions. For  $Y_{16}Fe_{29}$ , the  $\chi_M T$  decreases rapidly to the minimum value of  $9.52 \text{ cm}^3 \text{ K mol}^{-1}$  at 2 K due to the strong antiferromagnetic interaction between the iron ions.<sup>[28]</sup> The results revealed that the substitution of metal sites results in different magnetic coupling behaviour between Gd and Y-based compounds. For compounds 1–4 the magnetic behaviour is comparable to that observed in the reported  $Fe_{17}$  with the same central  $Fe_{13}$ -Keggin unit;<sup>[3a]</sup> the iron ions in the tetrahedral and octahedral holes are antiferromagnetically coupling. Only magnetic coupling of Fe...Fe exists in  $Y_{12}Fe_{33}$  and  $Y_{16}Fe_{29}$  because Y(III) is diamagnetic, but the weak ferromagnetic coupling paths of Gd...Gd and Gd...Fe are increased in  $Gd_{12}Fe_{33}$  and  $Gd_{16}Fe_{29}$ , thus leading to the different magnetic coupling behaviour between Gd- and Y-based compounds.

## Conclusions

Here we have isolated the  $\epsilon$ - $Fe_{13}$  Keggin cluster unit; the exact building block for magnetite, and a close approximation for the presumed (but debated) building block for ferrihydrite. The core Keggin structure is surrounded by 32 additional  $Fe^{3+}$  and  $Y^{3+}/Gd^{3+}$  polyhedra and capped by organic ligands. Both the rare earths and ligands stabilize the highly reactive iron-oxo core. Additionally, the terminal hydroxyls are preserved in the reported structures, a rare feature in aqueous metal-oxo clusters of all metal-ion types. Surrounding the  $\epsilon$ - $Fe_{13}$  core, the second shell of Fe-cations are also located in the identical positions as in magnetite. In this series of four isostructural compounds, the rare earths and Fe occupy the same positions, but all with slightly different arrangements in the outer metal-centres, presumably due to preference for different coordination sites of the different-sized Fe/Y/Gd ions. This suggests an entire family of compounds is possible, based on different ratios of Fe:Ln, and highlights opportunities to construct molecular forms of important magnetic materials. Moreover, these molecules provide unprecedented models for the rich geochemistry of lanthanides that are incorporated into ferrihydrite as impurities and alter transformation pathways to crystalline iron oxides. Future studies include expanding this class of molecular materials and using them for models to understand growth of ferrihydrite in the presence of rare earths in nature.

## Acknowledgements

This work was supported by the National Natural Science Foundation of China (Grants nos. 21871224, 21901002, 21673184, 21431005, and 21721001). We thank the staff from BL17B beamline of the National Center for Protein Sciences Shanghai (NCPSS) at the Shanghai Synchrotron Radiation Facility for their assistance during data collection and Dr. Zhenyi Zhang at Bruker (Beijing) Scientific Technology Co., Ltd. for help with the structure refinement. The SAXS analyses, interpretation and assistance in manuscript preparation performed at OSU by M.A. and M.N. was supported by the U.S. Department of Energy, Office of Basic Energy Sciences, Division of Material Sciences and Engineering, under award DE SC0010802.

## Conflict of interest

The authors declare no conflict of interest.

**Keywords:** Keggin · lanthanide-iron-oxo clusters · magnetite · Mössbauer spectroscopy · SAXS

- [1] a) G. P. Huffman, B. Ganguly, J. Zhao, K. R. P. M. Rao, N. Shah, Z. Feng, F. E. Huggins, M. M. Taghiei, F. Lu, *Energy Fuels* **1993**, *7*, 285–296; b) A. Lewin, G. R. Moore, N. E. Le Brun, *Dalton Trans.* **2005**, 3597–3610; c) D. G. Rancourt, D. Fortin, T. Pichler, P.-J. Thibault, G. Lamarche, R. V. Morris, P. H. J. Mercier, *Am. Mineral.* **2001**, *86*, 834–851; d) U. Schwertmann, L. Carlson, E. Murad, *Clays Clay Miner.* **1987**, *35*, 297–304; e) H. Deng, X. Li, Q. Peng, X. Wang, J. Chen, Y. Li, *Angew. Chem. Int. Ed.* **2005**, *44*, 2782–2785; *Angew. Chem.* **2005**, *117*, 2842–2845.
- [2] U. Schwertmann, R. M. Cornell, *The Iron Oxides: Structure, Properties, Reactions, Occurrence, and Uses*, Wiley-VCH, **2003**, pp. 1–137.
- [3] a) G. W. Powell, H. N. Lancashire, E. K. Brechin, D. Collison, S. L. Heath, T. Mallah, W. Wernsdorfer, *Angew. Chem. Int. Ed.* **2004**, *43*, 5772–5775; *Angew. Chem.* **2004**, *116*, 5896–5899; b) M. Evangelisti, A. Candini, A. Ghirri, M. Affronte, G. W. Powell, I. A. Gass, P. A. Wood, S. Parsons, E. K. Brechin, D. Collison, S. L. Heath, *Phys. Rev. Lett.* **2006**, *97*, 167202–167205.
- [4] a) H. Y. Huang, Z. Y. Chen, R. P. Wang, F. M. F. de Groot, W. B. Wu, J. Okamoto, A. Chainani, A. Singh, Z. Y. Li, J. S. Zhou, H. T. Jeng, G. Y. Guo, J. G. Park, L. H. Tjeng, C. T. Chen, D. J. Huang, *Nat. Commun.* **2017**, *8*, 15929–15934; b) M. B. Gawande, P. S. Branco, R. S. Varma, *Chem. Soc. Rev.* **2013**, *42*, 3371–3393; c) J. Kim, H. S. Kim, N. Lee, T. Kim, H. Kim, T. Yu, I. C. Song, W. K. Moon, T. Hyeon, *Angew. Chem. Int. Ed.* **2008**, *47*, 8438–8441; *Angew. Chem.* **2008**, *120*, 8566–8569.
- [5] a) A. Manceau, *ACS Earth Space Chem.* **2019**, *3*, 1576–1580; b) D. G. Rancourt, J. F. Meunier, *Am. Mineral.* **2008**, *93*, 1412–1417; c) F. Maillot, G. Morin, Y. Wang, D. Bonnin, P. Ildefonse, C. Chaneac, G. Calas, *Geochim. Cosmochim. Acta* **2011**, *75*, 2708–2720; d) D. Peak, T. Regier, *Environ. Sci. Technol.* **2012**, *46*, 3163–3168.
- [6] a) T. D. Waite, J. A. Davis, T. E. Payne, G. A. Waychunas, N. Xu, *Geochim. Cosmochim. Acta* **1994**, *58*, 5465–5478; b) T. A. Marshall, K. Morris, G. T. Law, F. R. Livens, J. F. Mosselmans, P. Bots, S. Shaw, *Environ. Sci. Technol.* **2014**, *48*, 3724–3731.
- [7] J. F. Banfield, S. A. Welch, H. Zhang, T. T. Ebert, R. L. Penn, *Science* **2000**, *289*, 751–754.
- [8] a) J. S. Weatherill, K. Morris, P. Bots, T. M. Stawski, A. Janssen, L. Abrahamsen, R. Blackham, S. Shaw, *Environ. Sci. Technol.* **2016**, *50*, 9333–9342; b) J. L. Jambor, J. E. Dutrizac, *Chem. Rev.* **1998**, *98*, 2549–2586.
- [9] O. Sadeghi, L. N. Zakharov, M. Nyman, *Science* **2015**, *347*, 1359–1362.
- [10] O. Sadeghi, C. Falaise, P. I. Molina, R. Hufschmid, C. F. Campana, B. C. Noll, N. D. Browning, M. Nyman, *Inorg. Chem.* **2016**, *55*, 11078–11088.

- [11] a) M. Sassi, K. M. Rosso, *ACS Earth Space Chem.* **2019**, *3*, 70–78; b) M. Sassi, C. I. Pearce, P. S. Bagus, E. Arenholz, K. M. Rosso, *J. Phys. Chem. A* **2017**, *121*, 7613–7618.
- [12] D. N. Woodruff, R. E. Winpenny, R. A. Layfield, *Chem. Rev.* **2013**, *113*, 5110–5148.
- [13] Y. Z. Zheng, G. J. Zhou, Z. Zheng, R. E. Winpenny, *Chem. Soc. Rev.* **2014**, *43*, 1462–1475.
- [14] a) D.-F. Weng, Z.-M. Wang, S. Gao, *Chem. Soc. Rev.* **2011**, *40*, 3157–3181; b) X. Y. Zheng, H. Zhang, Z. Wang, P. Liu, M. H. Du, Y. Z. Han, R. J. Wei, Z. W. Ouyang, X. J. Kong, G. L. Zhuang, L. S. Long, L. S. Zheng, *Angew. Chem. Int. Ed.* **2017**, *56*, 11475–11479; *Angew. Chem.* **2017**, *129*, 11633–11637.
- [15] a) A. Baniodeh, Y. Liang, C. E. Anson, N. Magnani, A. K. Powell, A.-N. Untereiner, S. Seyfferle, M. Slota, M. Dressel, L. Bogani, K. Goß, *Adv. Funct. Mater.* **2014**, *24*, 6280–6290; b) I. A. Gass, C. J. Milios, A. Collins, F. J. White, L. Budd, S. Parsons, M. Murrie, S. P. Perlepes, E. K. Brechin, *Dalton Trans.* **2008**, 2043–2053.
- [16] a) A. A. Abu-Nawwas, J. Cano, P. Christian, T. Mallah, G. Rajaraman, S. J. Teat, R. E. Winpenny, Y. Yukawa, *Chem. Commun.* **2004**, 314–315; b) Y. Sasaki, K. Umakoshi, S. Kimura, C.-E. Oh, M. Yamazaki, T. Shibahara, *Chem. Lett.* **1994**, *23*, 1185–1188.
- [17] J. Hua, C. Liu, F. Li, Z. Zhu, Z. Wei, M. Chen, T. Gao, G. Qiu, *ACS Earth Space Chem.* **2019**, *3*, 895–904.
- [18] W. B. Kamb, *Acta Crystallogr.* **1960**, *13*, 15–23.
- [19] a) U. Schwertmann, E. Murad, *Clays Clay Miner.* **1990**, *38*, 196–202; b) S. Ardizzone, A. Chittofrati, L. Formaro, *J. Chem. Soc. Faraday Trans. 1* **1987**, *83*, 1159–1168; c) P. S. Sidhu, R. J. Gilkes, A. M. Posner, *Soil Sci. Soc. Am. J.* **1980**, *44*, 135–138; d) R. Giovanoli, R. M. Cornell, *Z. Pflanzenernaehr. Bodenkd.* **1992**, *155*, 455–460; e) R. M. Cornell, R. Giovanoli, P. W. Schindler, *Clays Clay Miner.* **1987**, *35*, 21–28.
- [20] a) V. Mereacre, D. Prodius, Y. Lan, C. Turta, C. E. Anson, A. K. Powell, *Chem. Eur. J.* **2011**, *17*, 123–128; b) D. Schray, G. Abbas, Y. Lan, V. Mereacre, A. Sundt, J. Dreiser, O. Waldmann, G. E. Kostakis, C. E. Anson, A. K. Powell, *Angew. Chem. Int. Ed.* **2010**, *49*, 5185–5188; *Angew. Chem.* **2010**, *122*, 5312–5315.
- [21] X. Zuo, G. Cui, K. M. Merz, L. Zhang, F. D. Lewis, D. M. Tiede, *Proc. Natl. Acad. Sci. USA* **2006**, *103*, 3534–3539.
- [22] P. Moore, *J. Appl. Crystallogr.* **1980**, *13*, 168–175.
- [23] L. B. Fullmer, P. I. Molina, M. R. Antonio, M. Nyman, *Dalton Trans.* **2014**, *43*, 15295–15299.
- [24] D. C. Hutchison, R. D. Stern, M. R. Olsen, L. N. Zakharov, K. A. Persson, M. Nyman, *Dalton Trans.* **2018**, *47*, 9804–9813.
- [25] a) L. Y. Guo, H. F. Su, M. Kurmoo, C. H. Tung, D. Sun, L. S. Zheng, *J. Am. Chem. Soc.* **2017**, *139*, 14033–14036; b) L. G. Christie, S. Asche, J. S. Mathieson, L. Vila-Nadal, L. Cronin, *J. Am. Chem. Soc.* **2018**, *140*, 9379–9382.
- [26] J. van Slageren, P. Rosa, A. Caneschi, R. Sessoli, H. Casellas, Y. V. Rikitin, L. Cianchi, F. D. Giallo, G. Spina, A. Bino, A.-L. Barra, T. Guidi, S. Carretta, R. Caciuffo, *Phys. Rev. B* **2006**, *73*, 014422–014431.
- [27] A. K. Powell, S. L. Heath, D. Gatteschi, L. Pardi, R. Sessoli, G. Spina, F. Del Giallo, F. Pieralli, *J. Am. Chem. Soc.* **1995**, *117*, 2491–2502.
- [28] A. E. Dearle, D. J. Cutler, H. W. L. Fraser, S. Sanz, E. Lee, S. Dey, I. F. Diaz-Ortega, G. S. Nichol, H. Nojiri, M. Evangelisti, G. Rajaraman, J. Schnack, L. Cronin, E. K. Brechin, *Angew. Chem. Int. Ed.* **2019**, *58*, 16903–16906; *Angew. Chem.* **2019**, *131*, 17059–17062.

---

Manuscript received: October 10, 2019

Accepted manuscript online: November 11, 2019

Version of record online: January 9, 2020